Journal of Power Sources 186 (2009) 500–507

Contents lists available at ScienceDirect

Journal of Power Sources

journal homepage: www.elsevier.com/locate/jpowsour

From single cell model to battery pack simulation for Li-ion batteries

Matthieu Dubarry, Nicolas Vuillaume, Bor Yann Liaw*

Hawaii Natural Energy Institute, SOEST, University of Hawaii at Manoa, 1680 East-West Road, POST 109, Honolulu, HI 96822, USA

ARTICLE INFO

Article history:
Received 12 August 2008
Received in revised form 5 October 2008
Accepted 7 October 2008
Available online 22 October 2008

Keywords:
Battery pack model
Cell-to-cell variations
Equivalent circuit model
SOC
State of health
Intrinsic cell imbalance

ABSTRACT

A practical universal modeling and simulation approach is presented in this paper to show that accurate battery pack simulation can be achieved if cell-to-cell variations were taken into account. A generic equivalent circuit model was used in the approach with parameters deduced from cell testing with proper protocols, which could come from live cell monitoring in a control circuitry. Using a single cell model, which was validated against experimental data and demonstrated with validity of high accuracy in predicting cell performance, we showed that such a high accuracy in single cell model is essential for a high fidelity pack simulation. It is also important to derive statistical confidence intervals accurately from experiments to characterize intrinsic cell-to-cell variations in capacity and internal resistance, which need to be considered in the pack model. If parameters for each individual cell were correctly approximated and used in the pack model, the accuracy in the prediction of pack performance could be significantly improved.

1. Introduction

Rechargeable lithium batteries (RLB) have been considered the battery of choice for many mobile and portable applications. The availability, maturity, and cost advantages have made the RLB market growth highly anticipated. Increasingly sophisticated operation of the RLB from cells to packs is also expected. For reliable operation of RLB in these applications, it is becoming crucial to demand accurate control of the pack and life prediction. Enabling such a capability presents significant values to the industry and the consumers if enhanced reliability in battery performance can be realized. However, accurately predicting battery performance and service life remains very challenging. The ability to predict battery service life accurately is highly desirable to date. A successful development of such a capability can promote RLB market penetration greatly.

Battery modeling has made substantial progress in recent years; yet predicting battery service life remains problematic, especially for a battery pack, due to the lack of an established practice to achieve such a prediction. Even with significant improvements in computing power and software capability [1–8] since 1990s, such a predictive capability still immature at the present time. In contrast, more advanced experimental studies had allowed unprecedented characterizations of the interfacial behavior and the electrode materials, which have advanced the understanding of the cell degradation processes [9]. These advancements help us improve our modeling to a more realistic service life prediction. Therefore, an integrated battery testing and simulation capability to assist battery R&D and operation is considerably easier nowadays than a decade ago [10].

To enable battery performance and service life prediction we need to develop a high-fidelity computer simulation. Such modeling and simulation should bridge laboratory knowledge and real-life experience so we can use laboratory test results to predict battery performance in real life.

In this work, we present an effort that uses an equivalent circuit model (ECM) to develop a battery simulation tool for RLB, with intention to enhance the simulation capability from cell to a realistic simulation of a battery pack. This modeling approach is simple yet practical because it allows accurate prediction of battery performance using data collected in the laboratory at the present time [8], but with an expectation that it will be equally useful in the future with in-line cell monitoring. This modeling approach uses parameters derived from typical laboratory test protocols such as those used in charge and discharge regimes; therefore, this modeling tool can be very versatile to simulate single cell behavior with minimal characterization of the chemistry in detail. We shall describe how to develop an accurate single cell model (SCM) first and then discuss how to migrate to a pack model and simulation. Special attention was paid to the cell imbalance issue, arisen from cell-to-cell variations, that is traditionally difficult to be characterized and quantified. We showed how to use a lot of 100 commercial cells to define the variances in their make-ups and variations in their behavior. From such analyses, we developed a rationalized

* Corresponding author. Tel.: +1 808 956 2339; fax: +1 808 956 2336.
E-mail address: bliaw@hawaii.edu (B.Y. Liaw).

0378-7753/$ – see front matter © 2008 Elsevier B.V. All rights reserved.
doi:10.1016/j.jpowsour.2008.10.051

methodology to incorporate such individual cell characteristics as cell-dependent parameters in SCM for pack modeling, conducted pack simulation, and assessed agreement with the test data for validation.

2. Experimental

2.1. Cell characterizations

A lot of 100 AAA $LiCoO_2$ Li-ion cells have been purchased from a commercial vendor. These cells were surveyed by weight and conditioned with five conditioning cycles, which comprised four *C*/2 and one *C*/5 discharge regimes. During the conditioning, all cells were charged using the manufacturer's recommended algorithm (which is CC at *C*/2 followed by CV at 4.2 V with *C*/200 or 1/2 h cut-off). Each cell was discharged with the same current, which is based on the nominal capacity of 300 mAh for the calculation of the *C*/*n* rates (*n* represents the discharge duration in hours). The capacities for different *C* rates were thus measured with a Solartron 1470 test station or a Bio-Logic VMP3® system. After the five conditioning cycles the cells were charged to 50% SOC for storage. One of the cells in the lot (denoted as the "nominal sample cell", NSC) was subjected to additional cycling at *C*/25, *C*/5, *C*/3, *C*/1 (1*C*) and 2*C* to determine its performance as the "nominal" characteristics of the cells, which were then used to derive all necessary parameters for the SCM. After each charge or discharge regime, the cell was set to allow a 3-h relaxation (at open circuit and $I = 0$) for equilibration. We subsequently used the average potential of the charge and discharge curves obtained at *C*/25 as the *pseudo*-open circuit voltage (*pseudo*-OCV) for NSC, and the state of charge (SOC) is defined by the full capacity determined by the *C*/25 charge discharge cycle assuming that the cell is polarized close to its thermodynamic state with minimal polarization at this rate. Although such a *pseudo*-OCV vs. SOC curve is a close approximation to the real equilibrium OCV vs. SOC curve, the former is more convenient and practical to be used to infer SOC than the latter. Such a *pseudo*-OCV vs. SOC curve is accurate enough for the purpose of this analysis and modeling.

2.2. Single cell model (SCM)

The SCM is an ECM [11] written in MATLAB®, and battery simulation was performed by feeding the SCM with the derived parameters for NSC to give a nominal behavior of this chemistry. The ECM approach for SCM enjoys benefits from its correspondence directly with the complex impedance of the cell; therefore, the SCM can simulate battery performance from the monitoring of the cell operating and the ambient condition. In electrochemical impedance spectroscopy (EIS), we use equivalent circuit diagrams to analyze the data from the EIS measurements to interpret the behavior of the battery system. In contrast, in the ECM, we use the associated equivalent circuit diagram to emulate battery behavior. Fig. 1 presents an example of an ECM used in this study, where V_o is the *pseudo*-OCV vs. SOC curve dictated by the cell thermodynamics. In the kinetic aspects of the cell, we depict the cell internal resistance by two contributions: R_1 the ohmic contribution that comprises the contact resistance and the electrolyte conductive resistance usually considered constant as determined by the EIS; and, R_2 the faradaic contributions including the charge transfer resistance and the Warburg resistance in the conductive porous electrodes. Similar to R_1 it is also convenient to determine R_2 by the EIS measurements at the same time. In a practical application, performing the EIS measurements and equivalent circuit analysis is impractical in a cell. In addition, the impedance is often SOC and rate-dependent [11].

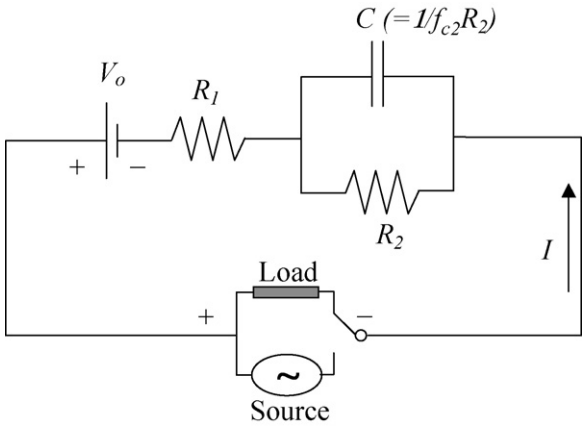

Fig. 1. Schematic of the equivalent circuit model (ECM) used in this work.

An alternative approach we considered is to derive R_2 from a simplified *pseudo*-Ohm's law, $V_{C/n} = I_{C/n}R_{exp}$, which serves as a first-order approximation of the cell kinetics. $V_{C/n}$ is the cell voltage response under *C*/*n* polarization with a current $I_{C/n}$. This approximation works well if the time step used is considerably smaller than the time constant of the associated reaction, thus the incremental change of the state is minimal. This simple approximation was used to determine the gross experimental resistance (R_{exp}) as a function of the SOC in this work. More precisely, we use the experimental data to derived R_{exp} from $\Delta V = R_{exp}\ \Delta I$ in a polarization regime. Using this approximation, we also estimated the *IR*-free voltage, which allowed us to project the OCV (V_{OC}), which was then used to infer the SOC that corresponds to this specific R_{exp}. So, in short, as long as we can determine a polarization voltage difference between two rates, we can estimate R_{exp} according to

$$\Delta V \Rightarrow V_{OC} - V_{C/n} = R_{\exp}(I_{OC} - I_{C/n}) \Leftarrow R_{\exp}\,\Delta I$$

whereas, $I_{OC} = 0$; and,

$$R_{\exp} = \frac{-(V_{OC} - V_{C/n})}{I_{C/n}}.$$

Using this simple scheme, we established the R_{exp} vs. SOC correspondence.

We should note that it is convenient to parameterize the resistance with normalization to the *C* rate, so there is no scaling issue when we compare batteries of different sizes. This normalized resistance R_{norm} (in Ω Ah) can be used in the model without knowing the actual current and the resistance R_{exp}:

$$R_{norm} = \frac{(V_{OC} - V_{C/n})}{C/n}$$

The normalized R_1 (R_{1_norm}) and R_2 (R_{2_norm}) can also be calculated by

$$R_{2\_norm} = R_{norm} - R_{1\_norm}$$

The distribution of the rated capacity among the cells allows us to perform a statistical analysis on the variance and standard deviation of the lot. Such a distribution for different rates, along with the distributions for weight and internal resistance, provides us an in-depth understanding of the nature of these distributions and their relationships with one another, whether correlated or not.

2.3. Battery pack simulation

For battery pack simulation, we developed methodologies and algorithms to modify parameters according to the variations in

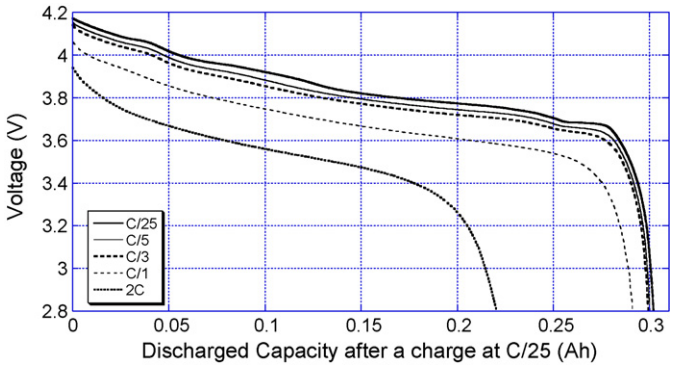

Fig. 2. Discharge curve (voltage vs. capacity) for the nominal sample cell (NSC) at *C*/25, *C*/5, *C*/3, *C*/1 and 2*C*.

capacity and internal resistance from one cell to another, so each individual cell in the pack retains its characteristics in the simulation. The battery pack model was developed in a Modelica® environment and compiled with the Dymola® engine [12]. We chose Modelica® over SIMULINK® because of the flexibility offered by Modelica® in modeling pack performance. The Modelica® is an open-source, object-oriented, multi-domain modeling language ideally for component-oriented modeling of complex systems such as those containing mechanical, electrical, electronic, hydraulic, thermal, control, electric power or process-oriented subcomponents. We used a "wired" topology and node connection to represent cells in a pack, and use Dymola® to solve equations for outputs according to the input parameters of the cells and conditions in the pack configuration. The topology also provides the flexibility in configuring the hierarchy of execution, which greatly facilitate the construction of a virtual test bench.

3. Results and discussion

3.1. Single cell modeling and validation

Fig. 2 presents the discharge curves of the NSC as a function of *C* rates, from *C*/25 to 2*C*. The cell was charged at *C*/25 prior to each discharge. Up to *C*/3 the cell can deliver close to the nominal rated capacity, whereas at 1*C* rate it loses about 3% of the rated *C*/2 capacity and 26% at 2*C*.

The common issue in cell testing and modeling is how to determine the SOC of the cell accurately. Since R_2 is a function of SOC, it should be derived from the subtraction of two different voltage vs. SOC curves, instead of voltage vs. capacity curves. To enable such a derivation, we have recently developed a method to correctly determine the SOC in a cell [13,14]. This method is based on an analysis of the cell relaxation voltage (equilibrium OCV) after each charge and discharge regime to allow precise determination of the terminal SOC for each charge discharge cycle at different *C* rates. In Fig. 3, the cell relaxation voltages are compared at (a) prior (i.e., after *C*/25 charge and before the discharge) and (b) after the discharge to the same cut-off voltage at different *C* rates. By correlating the cell relaxation voltage with the *pseudo*-OCV vs. SOC curve we were able to determine the terminal SOC before and after the discharge at different rates. Fig. 3(a) shows the relaxation voltages prior to discharge at different rates. These voltages are almost identical; as expected, since the cell has been charged at *C*/25 each time. In contrast, the cell relaxation voltages after discharging to the same end-of-discharge voltage (EODV = 2.75 V, as specified by the manufacturer) at different rates are different (Fig. 3(b)). For example, when the cell was discharged at 2*C* to EODV the depth of discharge (DOD, reflecting the amount of capacity delivered) only reached about 26% SOC. It is important to note that such a correspondence of DOD vs. SOC is very useful, in our view, to trace the cell's ability to deliver capacity through duty cycle polarization. It is also important to note that such a correspondence does not always follow SOC = 100% – DOD. In our previous work [13,14] we have explained the difference between the "thermodynamic" SOC (*t*-SOC) and "engineering" SOC (*e*-SOC, which by definition follows the convention of "100% – DOD"). The difference is that the *e*-SOC is based on "coulomb counting," while the *t*-SOC depends on "electrochemical equilibrium," which should be determined by OCV measurements. The *e*-SOC primarily reflects the kinetics of the cell, thus rate dependent; whereas the *t*-SOC concedes at equilibrium as a thermodynamic condition and therefore rate-independent. To properly address this difference, we shall use the following convention in this work: the SOC should correspond to the *t*-SOC, whereas DOD is represented by (100% – *e*-SOC) and denoted by the % of rated nominal capacity. To this end it is critical to point out that the *t*-SOC determined by correct OCV measurements will provide a true reference to the state of the battery. The *e*-SOC, on the other hand, cannot. By using *e*-SOC, one can conceive that various degrees of error at times will be introduced to the SOC estimate due to the lack of a reliable reference. Mistaking SOC = 100% – DOD could lead to a significant amount of accumulated error at the end of the simulation and greatly undermine the accuracy of the prediction.

With the terminal SOC determined by OCV measurements through cycles correctly, as shown in Fig. 3(b), we can display an accurate trace of the DOD-SOC correspondence with cycle num-

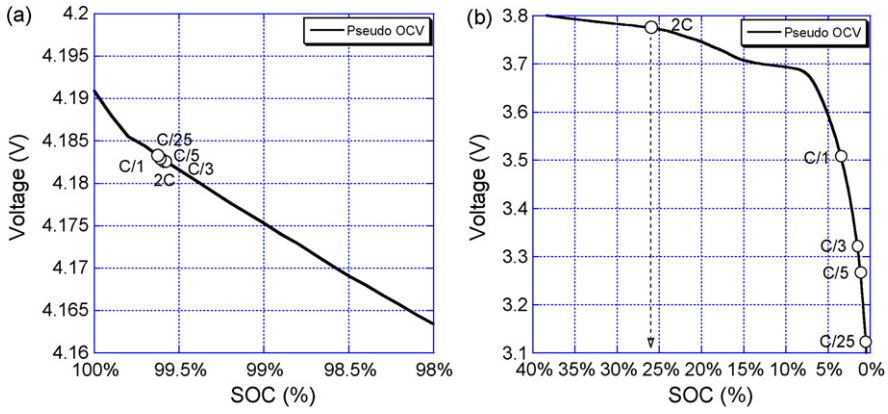

Fig. 3. *Pseudo*-OCV analysis reveals the cell discharge behavior. A comparison of the cell relaxation voltage vs. *pseudo*-OCV (a) prior to discharge and (b) after the relaxation in the post discharge rest periods at different *C* rates allows us to determine the corresponding SOC.

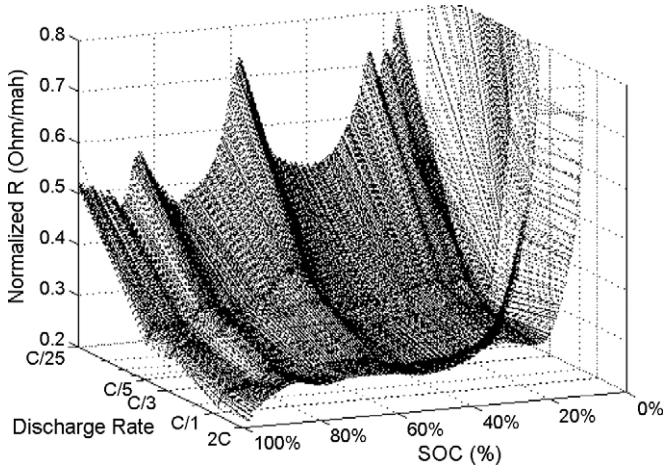

Fig. 4. Normalized resistance map associated with SOC at $C/25$, $C/5$, $C/3$, $C/1$ and $2C$ rates with linear extrapolation between sequential curves.

ber. This ability allows us to deduce normalized resistance from the cell voltage vs. SOC curves with cycle number. Such a protocol helps us to monitor the degradation of the cell in capacity loss with sufficient understanding of the changes in the terminal SOC cycle by cycle. Such a quantification of capacity loss can be used as an accurate method to estimate battery age and the state of health (SOH) through duty cycle aging. Fig. 4 presents a map correlating normalized resistance with SOC and the discharge C rate (at the initial state of the battery). The shape of the surface is dictated by the electrochemical processes, primarily transitions from one phase transformation to another in the cell, and is rate dependent. For instance, the resistance values close to 0% SOC increase noticeably. Such increases are governed by the last few staging processes in the graphite anode. A transition from one phase transformation to another often incurs in a solid solution, accompanied with a change in the Gibbs free energy associated with this transition, which leads to a noticeable potential change and thus reflected in the resistance. The shape is further influenced by the kinetics of either the Li intercalation in the solid solution or the phase transformation. For higher rates the changes in the shape are broadened and become less visible than those at the lower rates. We can yield a similar map for the rate effect of the charge regime as well.

In order to validate the SCM using the resistance-SOC-rate map in Fig. 4, we use the discharge curve at $C/2$ rate as an example. Such a $C/2$ discharge curve was simulated from the SCM using a resistance-SOC curve interpolated from Fig. 4, and the result is compared to the experimental data in Fig. 5. This $C/2$ rate data

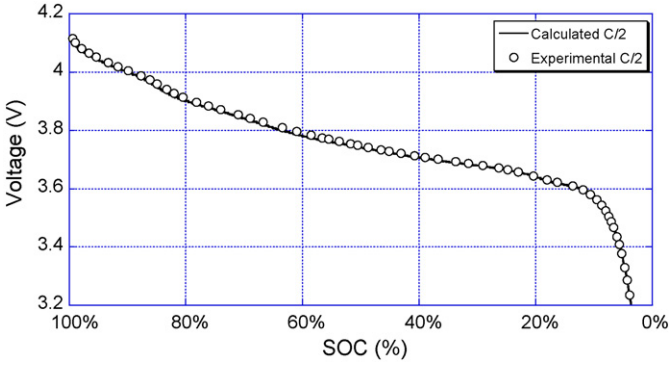

Fig. 5. SCM validation: experimental $C/2$ discharge data (○) compared to the simulated $C/2$ discharge curve.

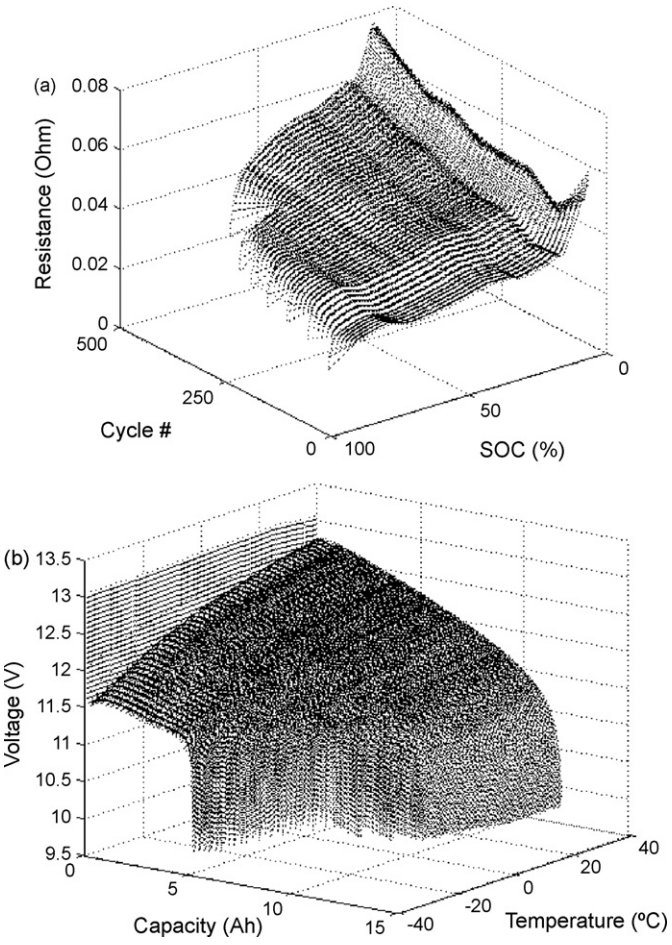

Fig. 6. (a) Resistance dependence on cycle history at $C/3$ discharge rate for a $LiFePO_4$-based Li-ion cell and (b) temperature-dependent voltage at $C/3$ discharge rate for a commercial lead acid module.

was not included in the matrix that was used to derive the map in Fig. 4. The standard deviation of the $C/2$ rate simulation is ±0.33% off the experimental data in average over the entire curve. Such agreement indeed illustrates the accuracy of the SCM with the resistance mapping technique and interpolation. Extrapolating the map beyond the envelope presented in Fig. 4 needs to be assessed cautiously. Operating the cell outside the specification (i.e., cell normal operating conditions) probably will induce additional adverse effects to the cell. One certainly would not expect the predictions could be validated with reliable data to assess the accuracy. It should be noted that such a high fidelity is crucial for pack simulation. As we will demonstrate later, cell-to-cell variations are a critical factor that strongly influences the pack performance. We shall call it "intrinsic cell imbalance." Without such a high fidelity SCM, intrinsic cell imbalance could not be quantified and simulated, nor can the pack performance be modeled with sufficient accuracy.

We would like to note that this ECM approach allows us to correlate the resistance R_{2_norm} with various parameters that are relevant to a specific application. For instance, maps can be obtained as a function of duty cycle regime, temperature, pressure, and then compiled into a multi-variant matrix/table for more complicated simulation. Such a complexity may lead to a more practical use in predicting battery behavior in the operations of aircraft instrumentation, space power, or deep ocean mooring. Fig. 6 presents an example of the maps obtained in (a) the resistance evolution with

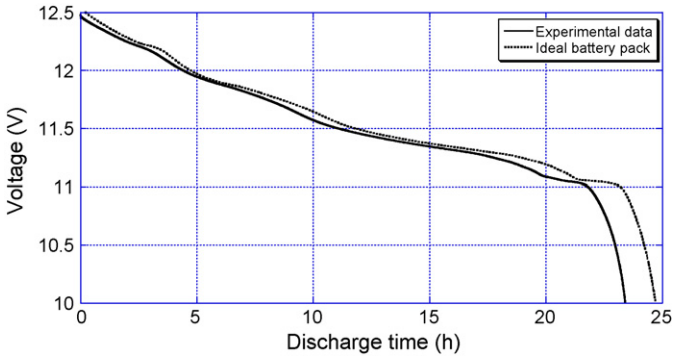

Fig. 7. Experimental data from a 3-cell string vs. the simulation of the string based on a generic SCM and make-up table of the NSC parameters.

duty cycle number for a commercial $LiFePO_4$-based Li-ion battery and (b) the temperature dependence of a lead acid battery module voltage. Both examples were obtained at *C*/3 rate.

3.2. From single cell model to battery pack simulation

3.2.1. Reality check on battery pack modeling

From a high fidelity SCM modeling to battery pack simulation, there are several issues need to be clarified before an accurate pack model can be realized. For instance, Fig. 7 presents a common issue experienced in a battery pack simulation originated from the variations in cell performance, as intrinsic cell imbalance. In this illustration, we compared the simulation and the experimental *C*/25 discharge curves of a battery string consisted of three cells in series (3S). In this simulation a generic SCM using the parameters derived from the NSC was used, with the assumption that the three cells were identical (i.e., no intrinsic cell imbalance). The three cells in the experiment were however consciously selected from the lot comprising one from each of the high, medium, and low capacity groups. In this trial, we found that the simulation (using the SCM with NSC parameters) yielded 6.5% more capacity than the experimental data of the 3S string. The prediction would be worsened to a greater degree with cycling. This experiment prompted us to conduct a more careful and thorough analysis on the variations in the cell performance in the lot and how they impact the pack performance. In order to understand such variations, the following analysis was performed.

3.2.2. Statistical analysis of a 100-cell lot

From the lot specification sheet provided by the vendor, the nominal capacity and the weight of the cells were supposed to be

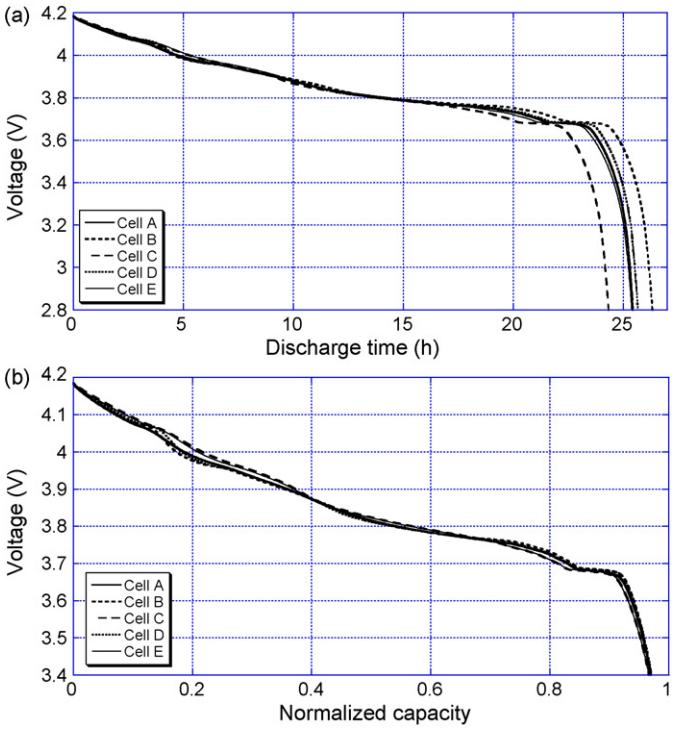

Fig. 9. (a) *C*/25 discharge (voltage vs. time) and (b) voltage vs. normalized capacity curves for five cells selected from the lot to show the disparities in the cell capacity.

300 mAh (based on a *C*/2 discharge) and 9 g, respectively. Upon surveying the cells, we found that ±1.9% and ±1.7% in variances in the *C*/2 capacity and weight were observed, respectively. In Fig. 8 we present the distributions of (a) the weight of the 100 cells in the lot and (b) the capacity at *C*/5 (with ±1.6% variance). The distributions may appear similar; but they do not seem to be directly correlated, since the cell-by-cell weight versus capacity correlation was not observed.

There are a number of possibilities that could lead to the observed discord in capacity and weight. Naturally, we can postulate that the difference in the active material content in the cells could result in the variance in the capacity. We attested this hypothesis experimentally as shown in Fig. 9. Fig. 9(a) displayed five *C*/25 discharge curves for five cells, noted as A to E, arbitrarily chosen in the lot. Again, although arbitrary, a conscious decision was made to choose the five that cover the entire range of the variance. It appears that with these five, there is a ±2.8% spread in the capacity variance. Fig. 9(b) displays the same information on a normalized capacity

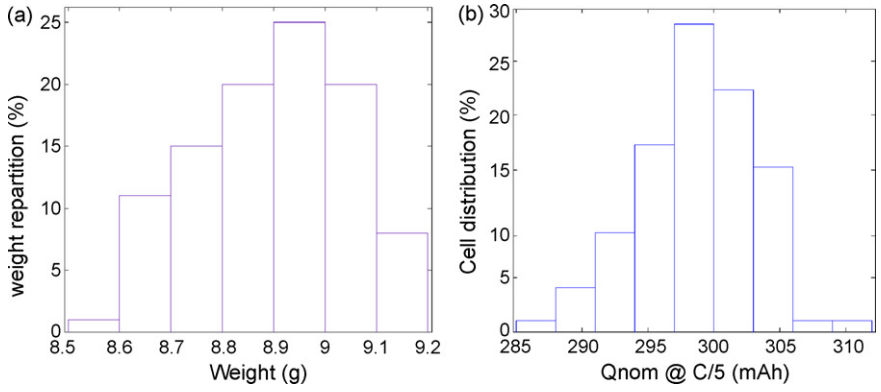

Fig. 8. Distribution of (a) the weight and (b) the *C*/5 nominal capacity of the 100 cells in the lot.

scale. The following analysis helped us understand the nature of this variance.

Since the variance in the cell capacity could come from either thermodynamic or kinetic origins, or both; it is important to separate kinetic contributions from the thermodynamic ones. Since the cells were discharged at *C*/25, we further assumed that the kinetic effects (as reflected in the polarization) could be minimized and negligible. Such an assumption was supported by the examination of the plateau voltages among the cells in Fig. 9(b). For instance, by comparing the last plateau voltage (before the EOD) among the five cells, we found that these plateau voltages are almost identical, substantiating our assumption that the polarization effects were truly negligible among the five; therefore, the polarization should have contributed little to the variance in the C_{25} capacity. It is then safe to suggest that the variance must come from some sort of thermodynamic origin. Next, we shall consider two possible types of variations: chemical or physical in nature. For chemical variations, no matter compositional variations in the active electrode material matrix or the amount of impurities, one would expect inevitable impacts on the electrochemical processes, shown as changes in the plateau range or reflected in the polarization. Fig. 9(b) shows that all the cells present the same electrochemical processes with similar potential and plateau range, indicating that there is little difference in the chemistry among the cells. This leads us to believe that the origins were physical in nature, possibly due to inhomogeneity in ink mixing and calendaring or deviation in the electrode footprint during cell fabrication. These physical attributes would then produce variations in capacity. It is therefore likely that we experienced variations in the content of the active material in the electrode among the cells.

We can further verify the above hypothesis by normalizing the discharge curve of each cell; thus determining a respective DOD according to its specific capacity in each cell. When the normalized discharge curves were presented in this manner, we found that the five curves indeed matched up quite consistently in Fig. 9(b), confirming our postulation that the variations in capacity were simply due to active material content in the cells. We further examined the relaxation cell voltages (similar to those in Fig. 3) and found that all the cells were indeed charged and discharged to the same terminal SOC under *C*/25. Therefore, we confirmed that the discrepancies in capacity among the five cells are most likely come from the differences in the amount of active material in the cells.

We should note that the difference in the active material content alone cannot explain the weight variations among the cells, and possibly, the variance in capacities at rates higher than *C*/25. There are other attributes that can lead to the disparities in the C_2 or C_5 capacities among the cells. These capacity disparities could involve kinetic origins.

A common problem we faced in testing multiple cells is that we often use the same current derived from the *C* rate based on the nominal capacity in the test for all the cells, disregarding their actual content in the active material. However, as a result of the different content in the active material in the cells, this constant current level in the test will not impose the same *C* rate for all cells anymore. Nor the current density will be the same. In other words, without imposing the same *C* rate on each cell, in correspondence to the specific amount of active material in each cell, it is inevitable that the test will result in the variations in the capacity. The situation gets worse as the *C* rate becomes higher.

There are other possibilities that can result in capacity variations at high rates from one cell to another. For instance, the contact resistance may vary from one cell to another. It suffices to say that variations in cell quality are a realistic concern, as we pointed out earlier regarding the uncorrelated disagreement between the weight and the active material content in the cell. Despite a variety of attributes that contribute to the cell performance variations, most of the kinetic contributions can be lumped into the "polarization" term. Interestingly, we further conducted an analysis to show that the variance in the polarization can be estimated to only about ±0.4% for the entire *C*/5 discharge regime (see Fig. 10), which is relatively small compared to capacity variations. We also should note that in certain regions of SOC where phase transition occurs, the polarization spread is higher (implying more sensitive to kinetics) than those in the plateaus, as shown in Fig. 10. Their impact on the capacity is however small.

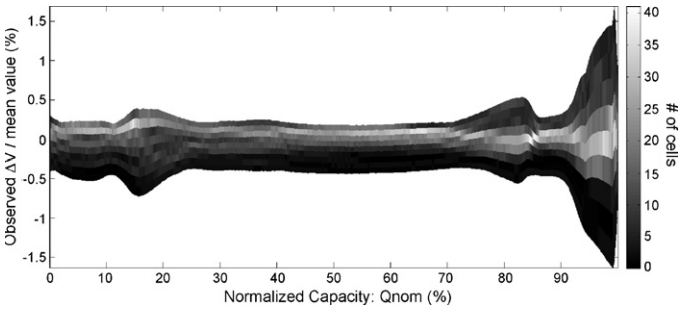

Fig. 10. A density plot showing the distribution of *C*/5 polarization and the mean value in the 100-cell lot.

Given all these analyses and considerations on different attributes to the capacity variations, we realized that no single attribute is sufficient to explain the 6.5% capacity discrepancy between the simulation and the actual experimental data, as shown in Fig. 7. If the discrepancy is truly an accumulated error from various attributes in the three-cell string, we need to improve the accuracy of the pack model to avoid "error-runaway" when the complexity of pack configuration increases. Otherwise, pack simulation and control will not be feasible and useful anymore.

3.2.3. Formulation of a pack model

It is conceivable now that the pack model has to take the intrinsic cell variations into consideration in the simulation. The nature of such an imbalance in the pack arisen from intrinsic cell variations, due to thermodynamic origins such as the variations in the active material content in the cell or kinetic origins represented by the polarization effects, needs to be reflected in the pack model and simulation.

Both thermodynamic and kinetic attributes can be depicted in the SCM as depicted in Fig. 11. These origins can be separated in the SCM to take into account of the intrinsic imbalance among the cells in the pack and be reflected in the model.

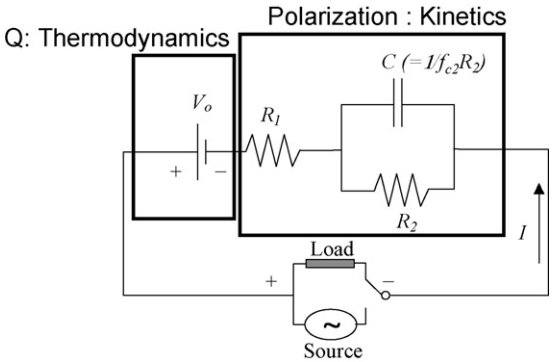

Fig. 11. Schematic of SCM with both thermodynamic and kinetic contributions incorporated.

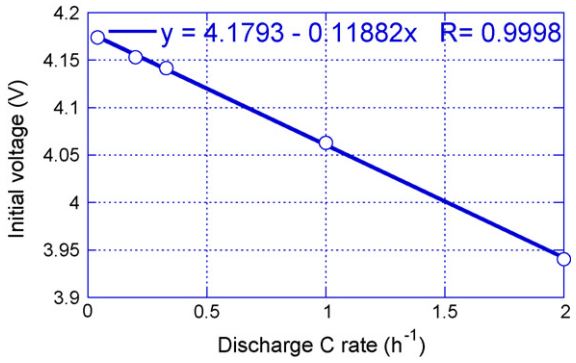

Fig. 12. Initial cell voltage (changed with the IR polarization upon imposition of current) vs. *C* rate for the NSC and a linear fit of the curve.

To properly take into account the variation of the capacity (which is related to the active material content), we need to properly scale the V_o – SOC correspondence in the SCM for each cell in the pack. Initially our definition of SOC is based on the C_{25} capacity for the NSC. For any other cell in the lot, the corresponding V_o – SOC needs to be scaled according to its capacity against that of the NSC.

To take into account the polarization effects, we noted that the variations in the polarization among the cells are a collective result from various resistive contributions—both ohmic and faradaic. To formulate a viable approach we analyzed possible variations in the normalized resistance map and developed a scheme to convert the polarization in each individual cell scaled to that of the NSC. The specific polarization parameters so determined for each cell were employed in the pack model to account for cell-to-cell variations in the simulation as follows.

First, we determined a "normalized polarization resistance" R_{np} in each cell by plotting the initial cell voltage (after the initial IR drop) versus the *C* rate. As shown in Fig. 12, we used the NSC as an example. The resulting curve is linear, as expected for a pseudo-ohmic behavior. A linear fit of the curve gives the slope and thus R_{np}, which is independent of current or *C* rate. For NSC, it is about 119 Ω Ah. Using the same technique, we can determine the unique R_{np} for each cell. By comparing the R_{np} of a specific cell versus that of the NSC (i.e., 119 Ω Ah), we yielded a scaling factor that can be used to convert the normalized resistance map for the NSC to a unique one for the specific cell. Therefore, each cell will have a unique normalized resistance map for the generic SCM to be used in the pack model.

This scaling process to derive the individual resistance map for each cell can be achieved in the conditioning cycles in which two different rates were applied. If more rates were employed in the conditioning, more accurate scaling of the resistance map can be accomplished.

Fig. 13 presents the variance of the polarization resistance from the 100 cells in the lot. Most of the cells exhibit resistance values within a narrow range close to that of the SNC. There are anomalies that could be related to contact problems, especially those on the high side.

3.2.4. Validation of the pack model

We have so far explained the analyses of the attributes to the cell variations in performance and the protocols to incorporate such disparities among the cells into the pack model and simulation. We shall now assess the effectiveness of these protocols in taking into account of the unique property of each cell and the intrinsic imbalance among the cells in the pack and quantify the improvement in accuracy of the pack model prediction.

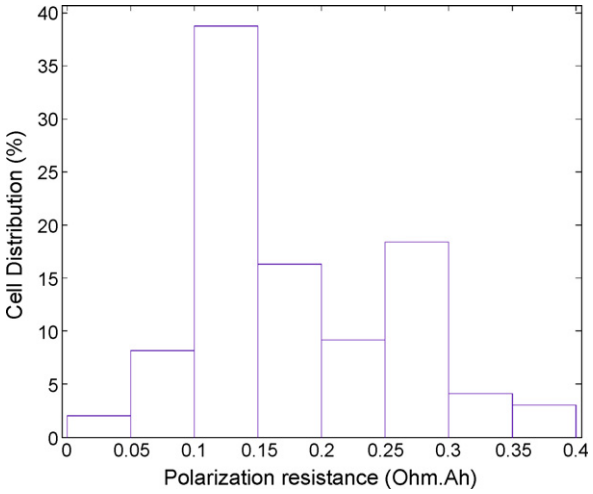

Fig. 13. Distribution of the polarization resistance among the 100 cells.

Returning to the previous three-cell string experiment, we now re-estimated the parameters for the three cells, namely cell 1/3, 2/3, and 3/3 (in the string configuration), as follows:

$$Q_{nom1/3} = 301\ \text{mAh},\ Q_{C/25\_1/3} = 307\ \text{mAh},\ R_{pol1/3} = 73\ \text{m}\Omega\ \text{Ah},$$

$$Q_{nom2/3} = 294\ \text{mAh},\ Q_{C/25\_2/3} = 301\ \text{mAh},\ R_{pol2/3} = 70\ \text{m}\Omega\ \text{Ah},$$

$$Q_{nom3/3} = 288\ \text{mAh},\ Q_{C/25\_3/3} = 295\ \text{mAh},\ R_{pol3/3} = 108\ \text{m}\Omega\ \text{Ah}.$$

Here the Q_{nom} is the C_2 capacity determined experimentally; while $Q_{C/25}$ is the capacity scaled from that of NSC. The C_{25} capacity of the string was simulated again with the newly scaled resistance map and V_o – SOC correspondence for each cell. Fig. 14 shows the comparison between the simulation and experimental data. The difference in the capacity prediction was reduced from the previous 6.5% to 1.6% with these protocols. The agreement in the cell voltage is also noticeably improved, particularly for the first 15 h in the discharge regime. In a closer examination of the individual cell data, we found that the behavior of the highest (1/3) and lowest capacity (3/3) cells was closely matched in the simulation, whereas the middle one (2/3) contributed to the majority of the discrepancy. It is important to point out that we have thus achieved a significant improvement in pack model accuracy, which is within the same confidence level of a cell; i.e., within 1.5–2%.

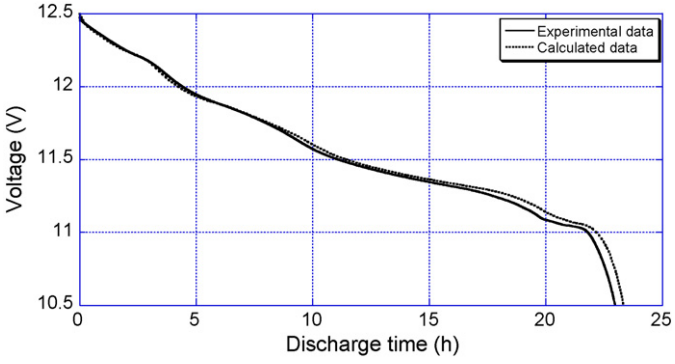

Fig. 14. Simulated discharge curve for the 3-cell string showed an improved accuracy with the consideration of intrinsic imbalance due to cell-to-cell variations.

3.2.5. Large pack modeling and simulation

Although the feasibility of treating intrinsic cell imbalance for a small string to achieve an accurate prediction in a pack has been demonstrated now, maintaining such accuracy as the cell number in the string increases remains to be validated. We however suspect that as the cell number increases, the degree of complexity to achieve accurate pack simulation also increases. The sensitivity to the initial cell imbalance could be more complicated as the cell number increases. An assessment on this hypothesis is in progress.

Our protocols will however allow us to detect such sensitivity in a quantitative manner. We are also looking for alternative analyses to help us reduce the burden of complexity in the simulation at the cell level so a validated technique can be developed to simplify the pack model prediction and improve accuracy. At the end, a simplified scheme can be used for parameterization for each cell according to the distribution and statistical confidence intervals to achieve a sufficient accuracy in the pack simulation. We are also assessing other contributions to the cell imbalance from external factors such as temperature gradient, thermal cycle induced effects, which should be considered in the pack model, so that the reality of operation and different degrees of impact on each cell can be incorporated in the pack model. After all, each protocol developed in this approach shall be able to contribute to a logical and systematic methodology to handle issues in the pack modeling.

4. Conclusion

We have shown that a simple and effective battery modeling approach using equivalent circuit technique can provide superior accuracy in predicting single cell performance, a comprehensive analysis on the issues related to the intrinsic cell imbalance, and improved accuracy in the battery pack performance simulation when cell-to-cell variations were taken into consideration. Therefore, this approach offers high fidelity simulations of the battery performance from a single cell to a pack, reflecting confidence level of a typical batch of cells and the manufacturer's quality in assembly. We rationalized the logic steps taken to achieve accurate predictions to battery pack performance. Attention was paid to the analysis of rate and SOC dependence of the polarization resistance in the cells to yield sufficient understanding of the attributes to the cell-to-cell variations in performance and quantify the intrinsic cell imbalance in a pack to permit accurate predictions at the pack level. We believe this is the first pack modeling and simulation with quantifiable identification of various attributes to cell performance variations in a lot to allow a proper incorporation of intrinsic cell imbalance into a pack model to achieve an unprecedented accuracy with the error contained within the distribution of a lot and validated with experiments.

Acknowledgements

This work was performed under a contract with the Hawaii Center for Advanced Transportation Technologies (HCATT, Contract # 54214) and with the support from the US Air Force Advanced Power Technology Office (APTO) at the Robins Air Force Base in Georgia.

References

[1] J. Newman, Electrochemical Systems, 2nd ed., Prentice Hall, Englewood Cliff, NJ, 1991.
[2] E. Barsoukov, J.H. Kim, J.H. Kim, C.O. Yoon, H. Lee, Solid State Ionics 116 (1999) 249–261.
[3] C. Fellner, J. Newman, J. Power Sources 85 (2000) 229–236.
[4] B. Wu, M. Mohammed, D. Brigham, R. Elder, R.E. White, J. Power Sources 101 (2001) 149–157.
[5] G.L. Plett, J. Power Sources 161 (2006) 1369–1384.
[6] R. Spotnitz, J. Power Sources 113 (2003) 72–80.
[7] P. Ramadass, B. Haran, P.M. Gomadam, R.E. White, B.N. Popov, J. Electrochem. Soc. 151 (2004) A196–A203.
[8] B.Y. Liaw, R.G. Jungst, G. Nagasubramanian, H.L. Case, D.H. Doughty, J. Power Sources 140 (2005) 157–161.
[9] FY2001 Annual Progress Report for the ATD Program, U.S. Department of Energy, Office of Transportation Technologies, <http://www.cartech.doe.gov/pdfs/B/196.pdf>.
[10] B.Y. Liaw, X.G. Yang, K.P. Bethune, Solid State Ionics 152/153 (2002) 51–59.
[11] M. Dubarry, B.Y. Liaw, J. Power Sources 174 (2007) 856–860.
[12] See <http://www.modelica.org/> and <http://www.dynasim.com/>. Additional information can be found at <http://en.wikipedia.org/wiki/Modelica>.
[13] M. Dubarry, V. Svoboda, R. Hwu, B.Y. Liaw, Electrochem, Solid State Lett. 9 (2006) A454–A457.
[14] M. Dubarry, B.Y. Liaw, J. Power Sources 174 (2007) 1121–1125.